Numerical simulation of energy states for vertically aligned quantum dots array by second order finite difference scheme

January 12, 2006

Abstract

We present a simple numerical method to investigate the electronic properties of a three-dimensional quantum dot array model formed by different size vertically aligned quantum dots. The corresponding Schrödin-ger equation is discretized using the finite difference method with a constant electron mass and confinement potential. The scheme is 2nd order accurate and converges extremely fast. In this paper, we propose numerical schemes to compute the energy levels of various QDA structures and research the existence of the anti-crossing and crossing eigencurve for QDA formed by two disk-shaped co-axial QDs with different size.

Keywords: Finite difference method, The Schrödinger equation, Energy levels, crossing eigencurve, anti-crossing eigencurve, quantum dot array.

1 Introduction

The quantum dot array (QDA) formed by vertically aligned semiconductor quantum dots (QDs) [36] among the various nanoscale hetrostructures. QDAs have been studied intensively in theory [26,27,31], experiment [5,10,24,29,32], and computation [8,9,14,15,16,22]. The further development applied by QDAs like QD computers [6,20], QD molecule [3], and QD laser [7,23].

Recently, the properties of a single-electron QDA heterostructure with a nonparabolic effective mass approximation have been studied numerically in

[14]. The paper assumes that a QDA is formed by identical size quantum dots and fine meshes are needed around the heterojunctions in the discretized scheme. The resulting numerical implementation of various size QDAs thus becomes very complicated.

In this paper, based on the finite volume scheme in [13,35], we propose a simple efficient uniform mesh scheme for various size QDAs over the cylindrical coordinate. The second order convergence rate of this scheme is numerically verified. Furthermore, some resulting numerical experiments are shown to explain the various physical phenomena of QDA.

The rest of the paper is organized as follows. We first describe the vertically aligned QDA model in Section 2, followed by the finite difference scheme simulating the QDA model in Section 3. Numerical simulation results and discussions are presented in Section 4. We conclude the paper in Section 5.

2 Vertically aligned quantum dot array

In this paper, we consider the QDA model that two vertically aligned disk-shaped coaxial InAs QDs are embedded in a cylindrical GaAs matrix as shown in Figure 1. In the model, the two QDs have different sizes. The notations R_j andh_j in Figure 1 denote the radius and height of j-th dot, respectively. The two QDs are separated by d_0 nm GaAs spacer layers. About works of disk-shaped (cylindrical) dots have been studied extensively in theory [17,19], in computation [21,22], and by experiments [2,4,25]. We consider the governing Schrödinger equation of the model in cylindrical coordinates,

$$-\frac{\hbar^2}{2m_i}\left[\frac{\partial^2 u}{\Delta r^2}+\frac{1}{r}\frac{\partial u}{\Delta r}+\frac{1}{r^2}\frac{\partial^2 u}{\Delta \theta^2}+\frac{\partial^2 u}{\Delta z^2}\right]+C_i u=\lambda u, \tag{1}$$

where $\hbar$ is the reduced Plank constant, λ is the total electron energy, $u(r,\theta,z)$ the corresponding eigenfunction, m_i and C_i are the electron effective mass and confinement potential, respectively, in the i-th region for i=1,2. Here 1-th and 2-th regions denote the QD and the matrix, respectively. For simplicity, we

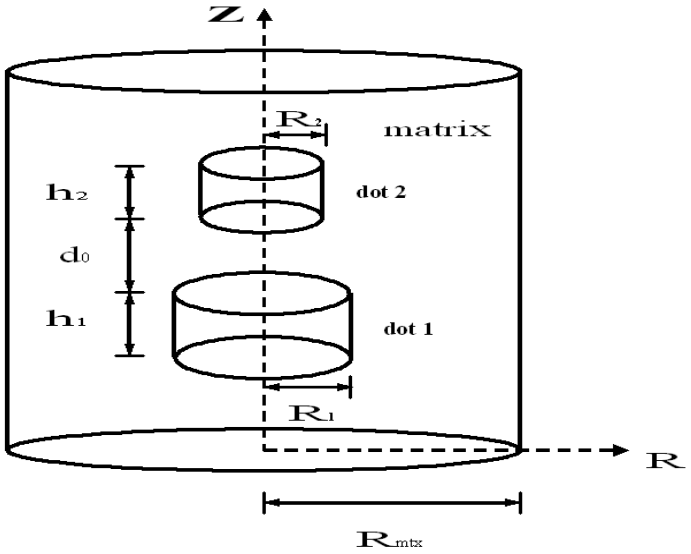

Figure 1: Structure schema of a cylindrical vertically aligned quantum dot array with variable size of the dot2 and the heterostructure matrix.

define $m^o \equiv \frac{\hbar^2}{2m_2}$, and $m^I \equiv \frac{\hbar^2}{2m_1}$. Then the Schrödinger equation (1) can be rewritten as follows

$$-m\left[\frac{\partial_r(r\partial_r u)}{r}+\frac{\partial_\theta^2 u}{r^2}+\alpha_z^2 u\right]+Cu=\lambda u, \tag{2}$$

where

$$m=\begin{cases} m^I & \text{in the dot,} \\ m^o & \text{in the matrix,} \end{cases} \qquad \text{and} \qquad C=\begin{cases} C^I=C_1 & \text{in the dot,} \\ C^o=C_2 & \text{in the matrix.} \end{cases} \tag{3}$$

For (2), Dirichlet boundary conditions,

$$u(r_B,\theta_B,z_B)=0 \tag{4}$$

are imposed on the boundary (top, bottom, and wall) of the matrix, where (r_B,θ_B,z_B) denotes the position on the matrix boundary.Moreover, the following BenDaniel-Duke boundary conditions are imposed on the interface:

$$m^I\frac{\partial u(r_I,\theta_I,z_I)}{\partial n_-}=m^o\frac{\partial u(r_I,\theta_I,z_I)}{\partial n_+}, \tag{5}$$

where (r_I, θ_I, z_I) denotes the position on the interface of the dot and the matrix, n_+ and n_- denote the corresponding outward normal derivatives of the interface that are defined for the matrix and dot regions, respectively.

Since the solution u is periodic in θ direction, we may rewrite (2) to transform the 3D problem to a sequence of 2D problems and gain significiant savings in computation. Let $\widehat{u}(r,z)$ be Fourier transform in θ directors of $u(r,\theta,z)$ that is

$$u(r,\theta,z) = \sum_l e^{il\theta}\widehat{u}(r,z), \tag{6}$$

where l is the Fourier mode. Since

$$\begin{aligned}\partial_\theta^2 u(r,\theta,z) &= -\sum_l l^2 e^{il\theta}\widehat{u}(r,z) \\ &= -l^2 u(r,\theta,z),\end{aligned} \tag{7}$$

we can rewrite (2) as

$$-m\left(\frac{\partial_r(r\partial_r\widehat{u})}{r} + \partial_z^2\widehat{u}\right) + \left(C + \frac{ml^2}{r^2}\right)\widehat{u} = \lambda\widehat{u}, \tag{8}$$

for a certain Fourier mode l. By using the above transformation, we only need to solve 2D problems for a certain Fourier mode to obtain all the eigenpairs that are of interest.

3 Finite difference scheme

In this section, we offer finite difference schemes for solving the 2D QDA Schrödinger equation (8). First we define L and M uniform mesh points along $r-$ and $z-$directions, respectively. Furthermore, Δr and Δz denote the mesh sizes, and the notation $u_{i,k}$ is used to represent the solution of Eq.(1) at the mesh point $(r_i,z_k)=((i-1/2)\Delta r, k\Delta z)$, for i=1,...,L and k=1,...,M.

We discretize the domain by choosing mesh points uniformly and half-integered in the radial direction to avoid incorporating the pole condition [31,32]. Figure 2 goes into detail about it.

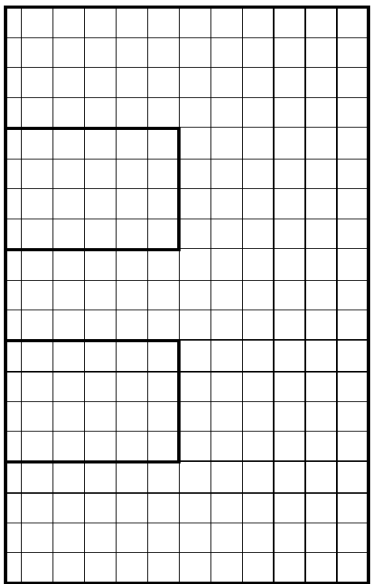

Figure 2: Schema of the uniform discretization scheme of a two-dot quantum dot array over a 2D half plane. Note that a half of the mesh length is shifted in the radial coordinate.

Consider the standard centered difference method for points in the interior and the exterior

$$
\begin{aligned}
&- m\left(\frac{r_{i+1/2}(u_{i+1,k}-u_{i,k})}{r_i(\Delta r)^2} - \frac{r_{i-1/2}(u_{i,k}-u_{i-1,k})}{r_i(\Delta r)^2} + \frac{u_{i,k+1}-2u_{i,k}+u_{i,k-1}}{(\Delta z)^2}\right) \\
&+ \left(C + \frac{ml^2}{r_i^2}\right) u_{i,k} = \lambda u_{i,k} \qquad (9)
\end{aligned}
$$

The finite difference scheme (9) can also be rearranged as

$$
\begin{aligned}
&\left(-\frac{m}{(\Delta z)^2}\right) u_{i,k-1} + \left(-\frac{mr_{i-1/2}}{r_i(\Delta r)^2}\right) u_{i-1,k} \\
&\quad + \left(\frac{m(r_{i-1/2}+r_{i+1/2})}{r_i(\Delta r)^2} + \frac{2m}{(\Delta z)^2} + C + \frac{ml^2}{r_i^2}\right) u_{i,k} \\
&\quad + \left(-\frac{mr_{i+1/2}}{r_i(\Delta r)^2}\right) u_{i+1,k} + \left(-\frac{m}{(\Delta z)^2}\right) u_{i,k+1} = \lambda u_{i,k} \qquad (10)
\end{aligned}
$$

Equation (9) can also be rearranged as

$$m\left(r_{i+1/2}\frac{u_{i+1,k}-u_{i,k}}{\Delta r}\Delta z - r_{i-1/2}\frac{u_{i,k}-u_{i-1,k}}{\Delta r}\Delta z\right)$$
$$+ m\left(r_i\frac{u_{i,k+1}-u_{i,k}}{\Delta z}\Delta r + r_i\frac{u_{i,k-1}-u_{i,k}}{\Delta z}\Delta r\right) = \left(r_i\lambda - Cr_i - \frac{ml^2}{r_i}\right)\Delta r\Delta z u_{i,k}, \tag{11}$$

which is a second order approximation of the integral form of the Schrödinger equation (2) over the control volume Ω of size $\Delta r \times \Delta z$

$$-\int_{\partial\Omega} m[(-r\partial_z u)dr + (r\partial_r u)dz] = \int\int_{\Omega}(\lambda r - Cr - \frac{ml^2}{r})u \tag{12}$$

as shown in (f) of Figure 3.

For the finite volume method in [13,35], the discretization of a grid point on the interface is based on the area of the intersection region of Ω and matrix. Under such discretized rules, the discretization of a grid point on the interface (a)-(e) in Figure 3 is derived as follows.

Case(i). The finite difference scheme on interface L as shown in(a) of Figure 3 is

$$\begin{aligned} &m^o\left(\frac{r_{i+1/2}}{r_i}\cdot\frac{u_{i+1,k}-u_{i,k}}{(\Delta r)^2}\right) + m^I\left(\frac{r_{i-1/2}}{r_i}\cdot\frac{u_{i,k}-u_{i-1,k}}{(\Delta r)^2}\right) \\ &\quad - \frac{m^I+m^o}{2}\left(\frac{u_{i,k+1}-2u_{i,k}+u_{i,k-1}}{(\Delta z)^2}\right) \\ &\quad + \left(\frac{C^o+C^I}{2} + \frac{m^I+m^o}{2}\cdot\frac{l^2}{r_i^2}\right)u_{i,k} = \lambda u_{i,k} \end{aligned} \tag{13}$$

which can be rearranged as

$$\begin{aligned} &\left(-\frac{m^I+m^o}{2(\Delta z)^2}\right)u_{i,k-1} + \left(-\frac{m^I r_{i-1/2}}{r_i(\Delta r)^2}\right)u_{i-1,k} \\ &\quad + \left(\frac{m^I+m^o}{r_i(\Delta r)^2}(r_{i-1/2}+r_{i+1/2}) + \frac{m^I+m^o}{(\Delta z)^2} + \frac{(m^I+m^o)l^2}{2r_i^2} + \frac{C^I+C^o}{2}\right)u_{i,k} \\ &\quad + \left(-\frac{m^o r_{i+1/2}}{r_i(\Delta r)^2}\right)u_{i+1,k} + \left(-\frac{m^I+m^o}{2(\Delta z)^2}\right)u_{i,k+1} = \lambda u_{i,k} \end{aligned} \tag{14}$$

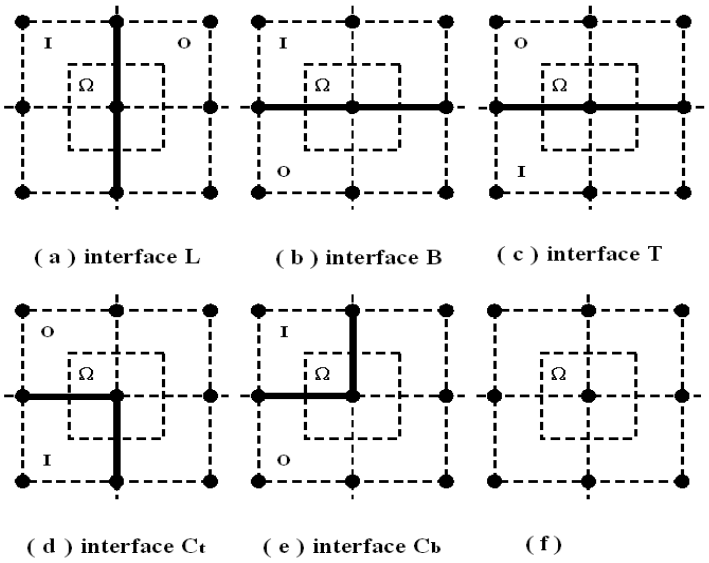

Figure 3: Discretization schema of the (a)left,(b)bottom,(c)top, (d)top corner,(e)bottom corner.The solid lines represents the heterojunctions. The solid points are the mesh points, where **I** and **O** are stood for inside and outside of the dot.

Case(ii). The finite difference scheme on interface B (Fig.3(b)) is

$$
\begin{aligned}
&-\frac{m^o+m^I}{2}\left(\frac{r_{i+1/2}}{r_i}\cdot\frac{u_{i+1,k}-u_{i,k}}{(\Delta r)^2}-\frac{r_{i-1/2}}{r_i}\cdot\frac{u_{i,k}-u_{i-1,k}}{(\Delta r)^2}\right)\\
&-m^I\left(\frac{u_{i,k+1}-u_{i,k}}{(\Delta z)^2}\right)+m^o\left(\frac{u_{i,k}-u_{i,k-1}}{(\Delta z)^2}\right)\\
&+\left(\frac{C^o+C^I}{2}+\frac{m^o+m^I}{2}\cdot\frac{l^2}{r_i^2}\right)u_{i,k}=\lambda ui,k
\end{aligned}
\tag{15}
$$

It can be rearranged as

$$
\begin{aligned}
&\left(-\frac{m^o}{(\Delta z)^2}\right)u_{i,k-1}+\left(-\frac{(m^I+m^o)r_{i-1/2}}{2r_i(\Delta r)^2}\right)u_{i-1,k}\\
&+\left(\frac{m^I+m^o}{2r_i(\Delta r)^2}(r_{i-1/2}+r_{i+1/2})+\frac{m^I+m^o}{(\Delta z)^2}+\frac{(m^I+m^o)l^2}{2r_i^2}+\frac{C^I+C^o}{2}\right)u_{i,k}\\
&+\left(-\frac{(m^I+m^o)r_{i+1/2}}{2r_i(\Delta r)^2}\right)u_{i+1,k}+\left(-\frac{m^I}{(\Delta z)^2}\right)u_{i,k+1}=\lambda u_{i,k}
\end{aligned}
\tag{16}
$$

Case(iii). on interface T (Fig.3(c)) we have

$$
\begin{aligned}
&-\frac{m^o+m^I}{2}\left(\frac{r_{i+1/2}}{r_i}\cdot\frac{u_{i+1,k}-u_{i,k}}{(\Delta r)^2}-\frac{r_{i-1/2}}{r_i}\cdot\frac{u_{i,k}-u_{i-1,k}}{(\Delta r)^2}\right)\\
&-m^o\left(\frac{u_{i,k+1}-u_{i,k}}{(\Delta z)^2}\right)+m^I\left(\frac{u_{i,k}-u_{i,k-1}}{(\Delta z)^2}\right)\\
&+\left(\frac{C^o+C^I}{2}+\frac{m^o+m^I}{2}\cdot\frac{l^2}{r_i^2}\right)u_{i,k}=\lambda ui,k
\end{aligned}
\tag{17}
$$

and rearrange as

$$
\begin{aligned}
&\left(-\frac{m^I}{(\Delta z)^2}\right)u_{i,k-1}+\left(-\frac{(m^I+m^o)r_{i-1/2}}{2r_i(\Delta r)^2}\right)u_{i-1,k}\\
&+\left(\frac{m^I+m^o}{2r_i(\Delta r)^2}(r_{i-1/2}+r_{i+1/2})+\frac{m^I+m^o}{(\Delta z)^2}+\frac{(m^I+m^o)l^2}{2r_i^2}+\frac{C^I+C^o}{2}\right)u_{i,k}\\
&+\left(-\frac{(m^I+m^o)r_{i+1/2}}{2r_i(\Delta r)^2}\right)u_{i+1,k}+\left(-\frac{m^o}{(\Delta z)^2}\right)u_{i,k+1}=\lambda u_{i,k}
\end{aligned}
\tag{18}
$$

Case(iv). The derivation for the discretization at the corner C_T(Fig.3(d)) is

$$
\begin{aligned}
&-m^o\left(\frac{r_{i+1/2}}{r_i}\cdot\frac{u_{i+1,k}-u_{i,k}}{(\Delta r)^2}\right)+\frac{m^I+m^o}{2}\left(\frac{r_{i-1/2}}{r_i}\cdot\frac{u_{i,k}-u_{i-1,k}}{(\Delta r)^2}\right)\\
&-m^o\left(\frac{u_{i,k+1}-u_{i,k}}{(\Delta z)^2}\right)+\frac{m^I+m^o}{2}\left(\frac{u_{i,k}-u_{i,k-1}}{(\Delta z)^2}\right)\\
&+\left(\frac{3C^o+C^I}{4}+\frac{3m^o+m^I}{4}\cdot\frac{l^2}{r_i^2}\right)u_{i,k}=\lambda u_{i,k}
\end{aligned}
\tag{19}
$$

Rearrange it as

$$
\begin{aligned}
&\left(-\frac{m^I+m^o}{2(\Delta z)^2}\right)u_{i,k-1}+\left(-\frac{(m^I+m^o)r_{i-1/2}}{2r_i(\Delta r)^2}\right)u_{i-1,k}\\
&+\left(\frac{m^I+m^o}{2(\Delta z)^2}+\frac{(m^I+m^o)r_{i-1/2}}{2r_i(\Delta r)^2}\right)u_{i,k}\\
&+\left(\frac{m^o r_{i+1/2}}{r_i(\Delta r)^2}+\frac{m^o}{(\Delta z)^2}+\frac{3C^o+C^I}{4}+\frac{(3m^o+m^I)l^2}{4r_i^2}\right)u_{i,k}\\
&+\left(-\frac{m^o r_{i+1/2}}{r_i(\Delta r)^2}\right)u_{i+1,k}+\left(-\frac{m^o}{(\Delta z)^2}\right)u_{i,k+1}=\lambda u_{i,k}
\end{aligned}
\tag{20}
$$

Case(v). At the corner C_B(Fig.3(e)) we have

$$
\begin{aligned}
&- m^o \left(\frac{r_{i+1/2}}{r_i} \cdot \frac{u_{i+1,k} - u_{i,k}}{(\Delta r)^2} \right) + \frac{m^I + m^o}{2} \left(\frac{r_{i-1/2}}{r_i} \cdot \frac{u_{i,k} - u_{i-1,k}}{(\Delta r)^2} \right) \\
&- \frac{m^I + m^o}{2} \left(\frac{u_{i,k+1} - u_{i,k}}{(\Delta z)^2} \right) + m^o \left(\frac{u_{i,k} - u_{i,k-1}}{(\Delta z)^2} \right) \\
&+ \left(\frac{3C^o + C^I}{4} + \frac{3m^o + m^I}{4} \cdot \frac{l^2}{r_i^2} \right) u_{i,k} = \lambda u_{i,k}
\end{aligned} \tag{21}
$$

and rearrange as

$$
\begin{aligned}
&\left(-\frac{m^o}{(\Delta z)^2} \right) u_{i,k-1} + \left(-\frac{(m^I + m^o) r_{i-1/2}}{2 r_i (\Delta r)^2} \right) u_{i-1,k} \\
&+ \left(\frac{m^I + m^o}{2(\Delta z)^2} + \frac{(m^I + m^o) r_{i-1/2}}{2 r_i (\Delta r)^2} \right) u_{i,k} \\
&+ \left(\frac{m^o r_{i+1/2}}{r_i (\Delta r)^2} + \frac{m^o}{(\Delta z)^2} + \frac{3C^o + C^I}{4} + \frac{(3m^o + m^I) l^2}{4 r_i^2} \right) u_{i,k} \\
&+ \left(-\frac{m^o r_{i+1/2}}{r_i (\Delta r)^2} \right) u_{i+1,k} + \left(-\frac{m^I + m^o}{2(\Delta z)^2} \right) u_{i,k+1} = \lambda u_{i,k}
\end{aligned} \tag{22}
$$

3.1 Jacobi-Davidson based algorithm for eigenvalue problem

Combining the finite difference discretizations of equations (10)-(22) results in the following eigenvalue problem:

$$
A\mathbf{u} = \lambda \mathbf{u}, \tag{23}
$$

where A is a sparse matrix with non-zero entries located in the main diagonal and four off-diagonals. The eigenvalue problem (23) can be solved by Jacobi-Davidson method [13] presented in Figure 4 to compute all of the desired eigenvalues.

4 Numerical results

In this section, we describe several numerical experiments to search the performance of our scheme. The experiments simulate the QD structure that an InAs QD is embedded in the GaAs cuboid. Following parameters are used in

Given a vector v_1 with $v_1^* v_1 = I$; set $V_1 = [v_1]$.
Compute $W_1 = AV_1$ and $M_1 = V_1^* W_1$.
Do $k = 1, 2, 3, \ldots$
(i) Iterate until convergence.
(ii) Compute all the eigenpairs of the small size problem
$$(M_k - \theta I_k)s = 0.$$
(iii) Select the desired (target) eigenpair (θ_k, s_k) and with $\| s_k \|_2 = 1$
(iv) Compute $u_k = V_k s_k$, and $r_k = (A - \theta_k I)u_k$.
(v) If $(||r_k||_2 < \varepsilon)$, Set $\lambda = \theta_k$, $x = u_k$, Stop.
(vi) Solve (approximately) a $t \perp u_k$ from
$(I - \frac{u_k u_k^*}{u_k^* u_k})(A - \theta_k I)t = -r_k$.
(vii) Orthogonalize t against V_k; Set $v_{k+1} = t / \| t \|_2$.
(viii) Compute $w_{k+1} = Av_{k+1}$, $M_{k+1} = \begin{bmatrix} M_k & V_k^* w_{k+1} \\ v_{k+1}^* W_k & v_{k+1}^* w_{k+1} \end{bmatrix}$,
(viii) Expand $W_{k+1} = [W_k, w_{k+1}]$ and $V_{k+1} = [V_k, v_{k+1}]$

Figure 4: Jacobi-Davidson Algorithm for solving $Au = \lambda u$.

our numerical simulation. The effective mass of InAs and GaAs are $0.024m_e$ and $0.0067m_e$, respectively. The confining potential for InAs and GaAs are 0.0 eV and 0.7 eV, respectively.

We implement the algorithms by using Fortran 90 programming language to manage numerical experiments. All the computations are executed on a workstation fitted with an Intel Itanium 900 MHz CPU and 12 GB main memory.

4.1 Second order convergence rate for single QD

In this subsection, we measure the convergence rate with a single QD which is embedded in a matrix. For such model, the height and the radius of the QD are 6 nm and 8 nm, respectively. For the matrix, the radius is assumed to be 16 nm. The matrix layers above the top and below the bottom of the QD are assumed to be the same as the QD height in our numerical experiments. We first check the convergence behavior of the discretization scheme, where the

matrix is partitioned into L, M meshes in each direction with Δr=$8/(L-1/2)$, Δz=$6/M$, and we choose Δr= Δz=h for convenience. As mesh refines, the rate of convergence on eigenvalues is measured by

$$rate_{[i]} = log_2 \left(\frac{\lambda_{[i]} - \lambda_{[i+1]}}{\lambda_{[i+1]} - \lambda_{[i+2]}} \right), \quad for \ i = 1, 2, 3 \tag{24}$$

where $\lambda_{[i]}$ for i=1,...,5 denote the approximate eigenvalues obtained from the meshes described in the table 1. Figure 5 illustrates the convergence rates ($rate_{[1]}$, $rate_{[2]}$, and $rate_{[3]}$) for the 12 target eigenvalues between 0 and 0.7. From the Figure 5, we find that all the convergence rates are close to 2 with a little differences.

(L-1,M-1)	Matrix dimension	Eigenvalue	Rate of convergence
(109,141)	15,369	$\lambda_{[1]}$	—
(219,283)	61,977	$\lambda_{[2]}$	—
(439,567)	248,913	$\lambda_{[3]}$	$rate_{[1]}$
(879,1135)	997,665	$\lambda_{[4]}$	$rate_{[2]}$
(1759,2271)	3994,689	$\lambda_{[5]}$	$rate_{[3]}$

Table 1: Matrix information for computing the rate of convergence, where L and M are the meshes in r-direction and z-direction of the matrix, respectively.

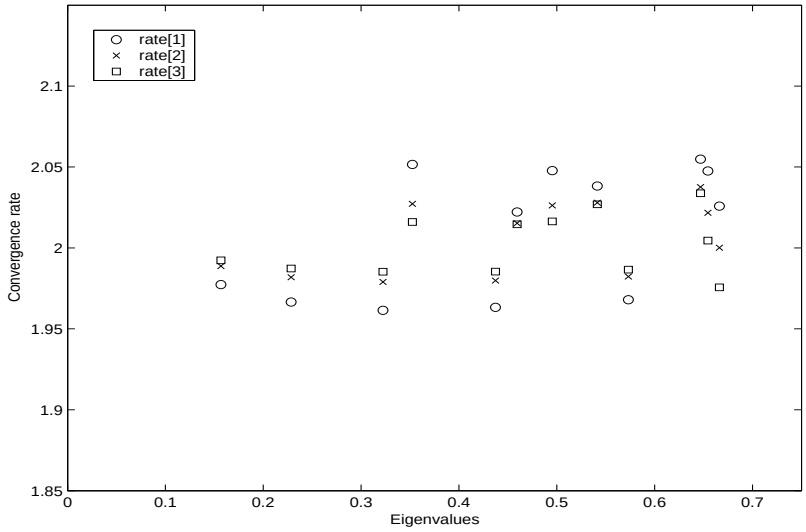

Figure 5: The 2nd convergent rate of eigenvalues which are between 0 and 0.7.

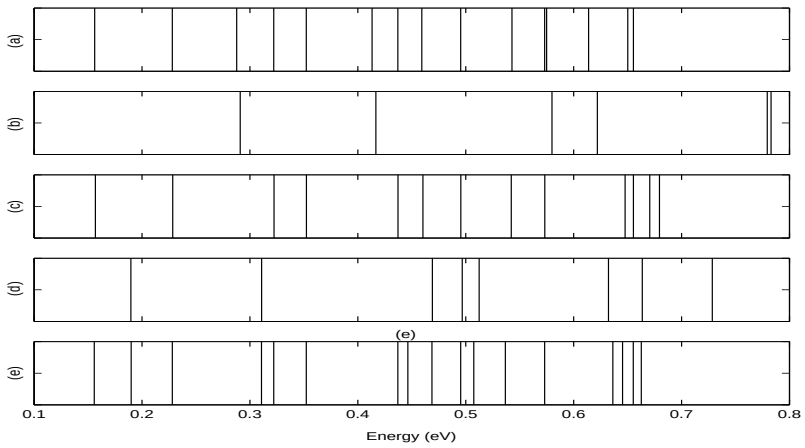

Figure 6: Energy spectrums of various QDA settings.The detail QDA structure parameters are given in Table2.

4.2 Energy levels of various QDA structures

All the energy spectrums of various QDA structures are illustrated in Figure 6 and the structure parameters, which include the dot width sizes (R) , height sizes (H),and gap distances, are listed in Table 2. Here, we consider the effect of pile up dots. The two-dot QDA structures in part (a) and (e) of Figure 6 are composed by the single-dot structures in (b) and (c), (c) and (d),respectively. Furthermore, the gap distances (D_{gap}) of (a) and (e) are both 3nm. For the QDAs as shown in (a) and (e), we have following two observations.

- The spectrums display in (a) and (e) of Figure 6 are rudely equivalent to the union of the single dot spectrums in (b) and (c), (c) and (d), repectively.

- The interaction among the energy levels are proposed in Figure 6-(a) and (e). For example, the energy levels that are greater than 0.6 eV in (a) and (e) are obtained from the interactions of the energy levels greater than 0.6 eV in (b) and (c), (c) and (d), respectively. In particular, such interactions are visible in the higher energy states.

	Figure 6 part	(a)	(b)	(c)	(d)	(e)
Two dots	R_1(nm)	8	-	-	-	8
	R_2(nm)	6	-	-	-	6
	H_1(nm)	6	-	-	-	6
	H_2(nm)	4	-	-	-	6
	D_{gap}(nm)	3	-	-	-	3
Single dot	R(nm)	-	6	8	6	-
	H(nm)	-	4	6	6	-

Table 2: The QDA structure parameters used in the numerical computation corresponding to the energy spectrums shown in Figure 6.

4.3 Bifurcation diagram of energy levels

In this subsection, we explore the occurrence of the QDAs by displaying the bifurcation diagram of energy levels versus the size of the quantum dots and the minimal difference of eigencurves in the anti-crossing(the distance of two different eigencurve is short) and crossing areas(the gap of two different eigencurve equals zero) in the various bifurcation diagrams. Specifically, we suppose that the size of the bottom QD is fixed to R_1=8 nm and H_1=6 nm. Then we compute the eigenvalues of the QDA by changing R_2 from 2 to 8 nm and H_2 from 0 to 6 nm. The results are shown in Figure 7 for space layer D_{gap} equals 6 and 9 nm in sub-figures (a) and (b), respectively. In addition, the eigenvalues computing results shown in Figure 8 is about the size of the bottom QD fixed to R_1=8 nm and H_1=6 nm; and the height of the top QD H_2=6 nm for space layer D_{gap} equals 3 and 6 nm in sub-figures (a) and (b), respectively. Here, we only plots the eigenvalue curves with the Fourier mode l=0 to illustrate the behavior in a clear manner.

Now we explain how the dot gap D_{gap} affect the "minimal energy gap" in the anti-crossing and crossing areas. We define $d(\lambda_i,\lambda_j,\underline{R}_2,\overline{R}_2)$ for the minimal energy gap(minimal difference of two eigencurve) in a certain range of R_2 (e.g. $\underline{R}_2 \leq R_2 \leq \overline{R}_2$ for pre-defined lower($\underline{R}_2$) and upper($\overline{R}_2$) bound of R_2), that is

$$d(\lambda_i, \lambda_j, \underline{R}_2, \overline{R}_2) = min\big\{|\lambda_i - \lambda_j|, for \underline{R}_2 \leq R_2 \leq \overline{R}_2\big\} \tag{24}$$

where λ_i is the ith eigenvalue of the QDA with a certain R_2. Here, we compute $d(\lambda_2,\lambda_3,5,6)$ in Fig. 9, $d(\lambda_3,\lambda_4,4,5)$ in Fig. 10 and $d(\lambda_4,\lambda_5,6.5,8)$ in Fig. 11 when R_1 and h_1 are fixed, R_2 and h_2 are changed at the same time. Similarly, we compute $d(\lambda_2,\lambda_3,2,4)$ in Fig. 12 and $d(\lambda_3,\lambda_4,6,8)$ in Fig. 13 when R_1, h_1 and h_2 are fixed, R_2 is changed. From Figure 9 to Figure 13, we can find that larger gap distance results in smaller minimal energy gap.

Moreover, Figure 11 has also implied that the eigencurves would become crossing (energy gap is zero) provided the two QDs are sufficiently far awary from each other. Similar results can be obtained in Figure 9 , Figure 10, Figure 11 and Figure 12 if we continue the computation by letting D_{gap} increases. Therefore, we have found that the QDAs with two different size co-axial QDs may result in anti-crossing eigencurves. If the two different size QDs are fixed and they are far away enough from each other, only crossing eigencurves are found. However, when the QDs are getting closer, the crossing points gradually become anti-crossing starting from higher energy levels.

5 Conclusion

In this article, we propose a 2nd order finite difference scheme to discretize the Schrödinger equation with uniform mesh at the QDA form by various size QDs. The relevant eigenvalues, which are embedded in the interior of the matrix eigenvalue spectrum, are solved successively using a Jacobi-Davidson based method. Numerical result also shows that the overall scheme is stable and efficient.

Our numerical experiments have displayed the existence of the anti-crossing and crossing eigencurve in the specific QDA structures at the QDA formed by two disk-shaped co-axial QDs with different size and anti-crossing can be found when the top QD is close enough to the bottom QD. Moreover, we have also studied the energy gap behaviors in the anti-crossing and crossing areas.

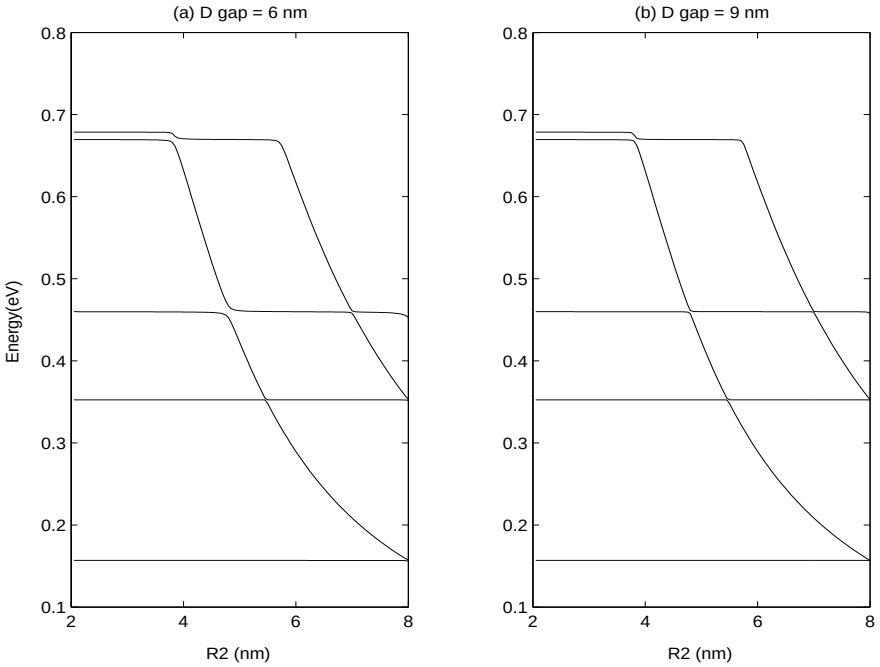

Figure 7: Bifurcation diagram of energy levels versus the size of the quantum dots. The bottom QD is fixed as R_1=8 nm and H_1=6 nm. The top dot size R_2 is changed from 2 to 8 nm, and H_2 is changed from 0 to 6 nm. The spacer layer distance D_{gap} equals 6 and 9 nm in sub-figures (a) and (b), respectively.

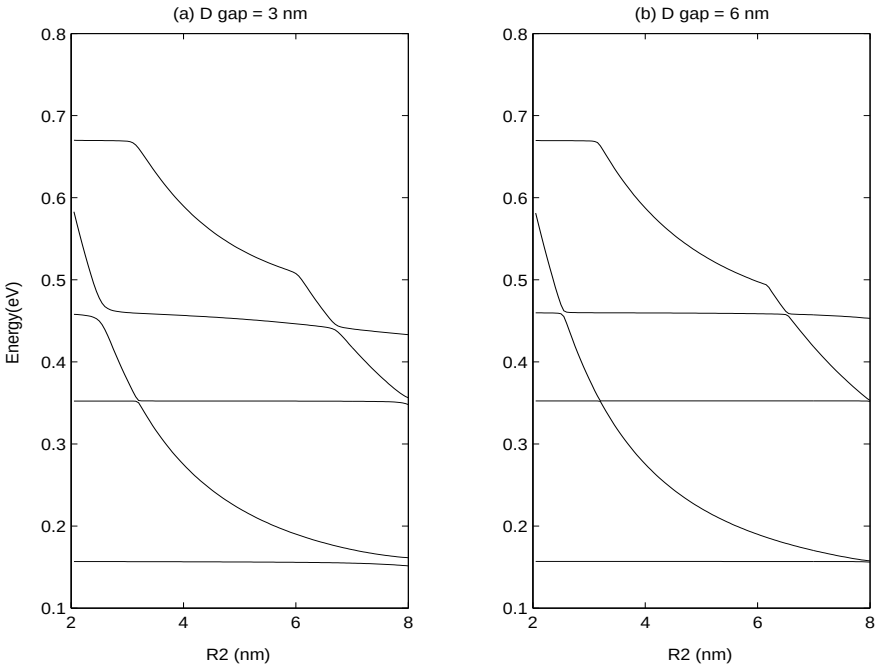

Figure 8: Bifurcation diagram of energy levels versus the size of the quantum dots. The bottom QD is fixed as R_1=8 nm and H_1=6 nm. The height of the top QD is fixed as H_2=6 nm.The top dot size R_2 is changed from 2 to 8 nm. The spacer layer distance D_{gap} equals 3 and 6 nm in sub-figures (a) and (b), respectively.

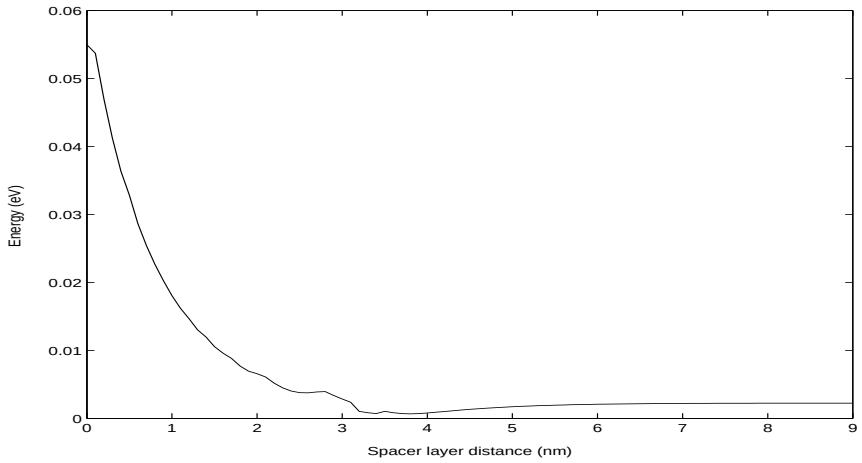

Figure 9: Changes of minimal energy gap in crossing area of $d(\lambda_2,\lambda_3,5,6)$ for D_{gap} changes from 0 to 9 nm.

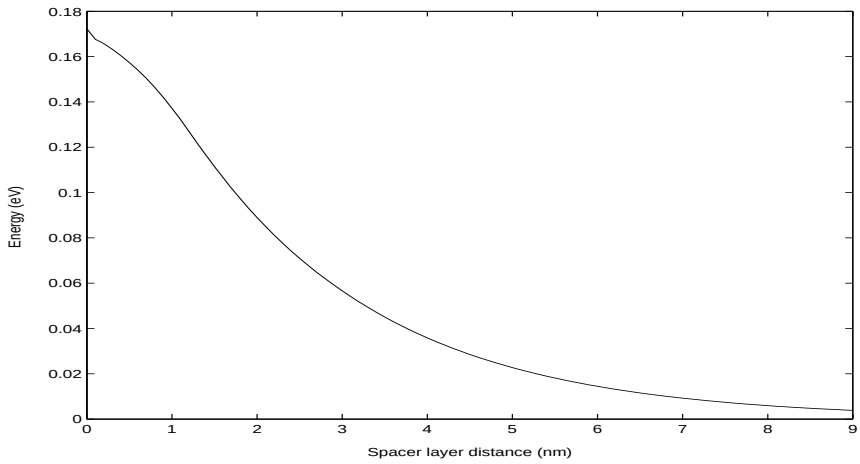

Figure 10: Changes of minimal energy gap in anti-crossing area of $d(\lambda_3,\lambda_4,4,5)$ for D_{gap} changes from 0 to 9 nm.

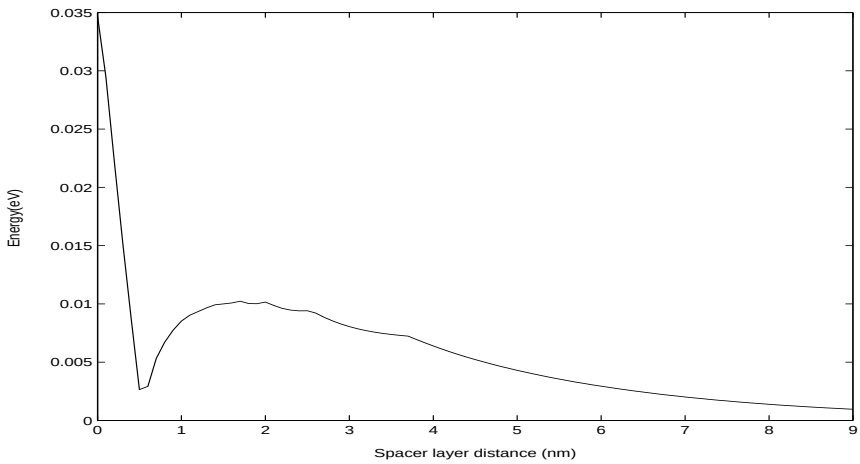

Figure 11: Changes of minimal energy gap in anti-crossing area of $d(\lambda_4,\lambda_5,6.5,8)$ for D_{gap} changes from 0 to 9 nm.

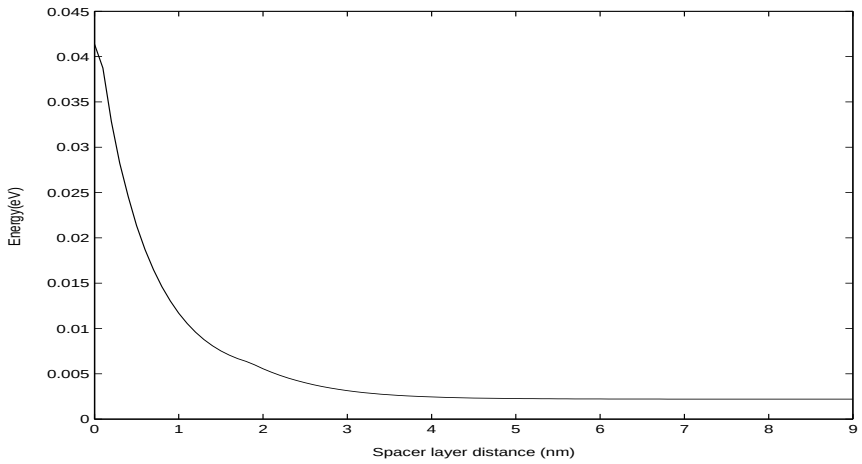

Figure 12: Changes of minimal energy gap in crossing area of $d(\lambda_3,\lambda_2,2,4)$ for D_{gap} changes from 0 to 9 nm.

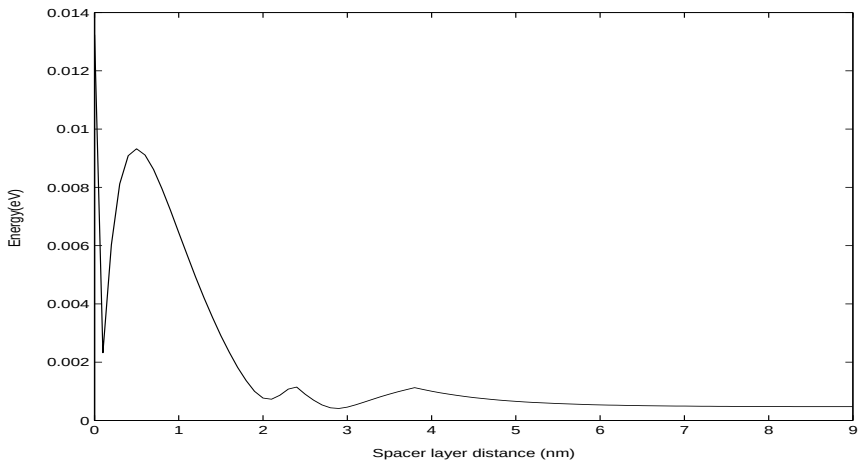

Figure 13: Changes of minimal energy gap in crossing area of $d(\lambda_3,\lambda_4,6,8)$ for D_{gap} changes from 0 to 9 nm.

References

[1] E.A. de Andrada e Silva, G.C. La Rocca and F. Bassani, Optical transition energies for lead-salt semiconductor quantum wells, *Phys. Rev. B* 60(12), 8859, (1999).

[2] D.G. Austinga, Y. Tokura and S. Tarucha, Addition energy spectrum of a quantum dot disk up to the third shell, *Physica E* 11, 63-67, (2001).

[3] M. Bayer, P. Hawrylak, K. Hinzer, S. Fafard, M. Korkusinski,Z.R. Wasilewski, O. Stern, and A. Forchel, Coupling and entangling of quantum dot molecules, *Science* , 451-453, (2001).

[4] M. Bayer, O. Schilling, A. Forchel, T.L. Reinecke, P.A. Knipp, Ph. Pagnod-Rossiaux and L. Goldstein, Splitting of electronic levels with positive and negative angular momenta in $In_{0.53}Ga_{0.47}As/InP$ quantum dots by a magnetic field, *Phys. Rev. B*, 15810-15814,(1996).

[5] R.H. Blick, D. Pfannkuche, R.J. Haug, K.V. Klitzing and K. Eberl, Formation of a coherent mode in a double quantum dot, *Phys. Rev. Lett.* 80, 4032-4035, (1998).

[6] G. Burkard, G. Seelig and D. Loss, Spin interactions and switching in vertically tunnel-coupled quantum dots, *Phys. Rev. B* 62, 2581-2592, (2000).

[7] S. Fafard, Z.R. Wasilewski, C.Ni. Allen, K. Hinzer, J.P.McCaffrey and Y. Feng, Lasing in quantum-dot ensembles with sharp adjustable electronic shells, *Applied Physics Letters* 75, 986-988, (1999).

[8] L.R.C. Fonseca, J.L. Jimenez and J.P. Leburton, Electronic coupling in InAs/GaAs self-assembled stacked double-quantum-dot systems, *Phys. Rev. B* 58, 9955-9960, (1998).

[9] F. Gelbard and K.J. Malloy, Modeling quantum structures with the boundary element method, *Journal of Computational Physics* 172, 19-39, (2001).

[10] H. Heidemeyer, S. Kiravittaya, C. Muller, N.Y. Jin-Phillipp and O.G Schmidt, Closely stacked InAs/GaAs quantum dots grown at low growth rate, *Applied Physics Letters* 80, 1544-1546, (2002).

[11] T.-M. Hwang, W.-W. Lin, J.-L. Liu and W.Wang, Fixed point methods for a semiconductor quantum dot model, *Mathl. Comput. Modelling* 40(5/6), 519-533, (2004).

[12] T.-M. Hwang and W.Wang, Analyxing and visualizing a discretized semilinear elliptic problem with Neumann boundary conditions, *Numer. Methods Partial Differ.Equ.* 18(3), 261-279, (2002).

[13] T.-M. Hwang, W.-W. Lin, W.-C. Wang and W.Wang, Numerical simulation of three dimensional pyramid quantum dot, *Journal of Computational Physics* 196, 208-232, (2004)

[14] T.-M. Hwang and W.Wang, Energy states of vertically aligned quantum dot array with nonparabolic effective mass, *Computers and Mathematics with Applications* 49, 39-51, (2005)

[15] T.-M. Hwang, W.Wang and W.-H.Wang, Numerical methods and findings for different size vertically aligned quantum dot array, *accepted Computer Physics Communications*

[16] H.T. Johnson, V. Nguyen and A.F. Bower, Simulated self-assembly and optoelectronic properties of InAs/GaAs quantum dot arrays,*Journal of Applied Physics* 92, 4653-4663, (2002).

[17] M. Korkusiski and P. Hawrylak, Electronic structure of vertically stacked self-assembled quantum disks, *Phys. Rev. B* 63, 195311, (2001).

[18] M.-C. Lai, A note on finite difference discretizations for Poisson equation on a disk, *Numer. Methods Partial Differ.Equ.* 17(3), 199-203, (2001).

[19] S. Le Goff and B. Stébé, Influence of longitudinal and lateral confinements on excitons in cylindrical quantum dots of semiconductors, *Phys. Rev. B* 47, 1383-1391, (1993).

[20] R. Leon, S. Fafard, P.G. Piva, S. Ruvimov and Z. Liliental-Weber, Tunable intersublevel transitions in self-forming semiconductor quantum dots, *Phys. Rev. B* 58, R4262-R4265, (1998).

[21] Y.Li,O. Voskoboynikov, C.P. Lee and S.M. Sze, Calculation of induced electron states in three-dimensional semiconductor artificial molecules, *Computer Physics Communications* 147, 209-213, (2002).

[22] R.V.N. Melnik and K.N. Zotsenko, Computations of coupled electronic states in quantum dot/wetting layer cylindrical structures, In *Computational Science*-ICCS 2003, (Edited by P. Sloot, D. Abramson, A. Bogdanov, J. Dongarra, A. Zomayz, and Y. Gorbachev), pp. 343-349, Springer-Verlag, (2003).

[23] M.V. Maximov, Yu.M. Shernyakov, A.F. Tsatsul'nikov, A.V. Sakharov, V.M. Ustinov, A.Yu. Egorov, A.E. Zhukov, A.R. Kovsh, P.S. Kop'ev, L.V. Asryan, Zh.I. Alferov, N.N. Ledentsov, D. Bimberg, A.O. Kosogov and P. Werner, High-power continuous-wave operation of a InGaAs/AlGaAs quantum dot laser, *Journal of Applied Physics* 83, 5561-5563, (1998).

[24] M.A. Migliorato, L.R. Wilson, D.J. Mowbray, M.S. Skolnick, M. Al-Khafaji , A.G. Cullis and M. Hopkinson, Structural and optical studies of vertically aligned InAs/GaAs self-assembled quantum dots, *Journal of Applied Physics* 90, 6374-6378, (2001).

[25] K. Ono, D.G. Austinga, Y. Tokura and S. Tarucha, Angular momentum selectivity in tunneling between two quantum dots, *Physica B* 314, 450-454, (2002).

[26] J.J. Palacios and P. Hawrylak, Correlated few-electron states in vertical double-quantum-dot systems, *Phys. Rev. B* 51, 1769-1777, (1995).

[27] C. Pryor, Quantum wires formed from coupled InAs/GaAs strained quantum dots, *Phys. Rev. Lett.* 80, 3579-3581, (1998)

[28] Th. Schapers, G. Engels, J. Lange, Th. Klocke, M. Hollfelder and H. Luth, Effect of the heterointerface on the spin splitting in modulation doped $In_{(x)}Ga_{(1-x)}$ As/InP quantum wells for b $\rightarrow$ 0 , *J. Appl. Physi.* 83(8), 4324, (1998).

[29] G. Schedelbeck, W. Wegscheider, M. Bichler and G. Abstreiter, Coupled quantum dots fabricated by cleaved edge overgrowth: From artificial atoms to molecules, *Science* 278, 1792-1795, (1997).

[30] G. Sek, K. Ryczko, J. Misiewicz, M. Bayer, F. Klopf, J.P. Reithmaier and A. Forchel, Photoreflectance spectroscopy of vertically coupled InGaAs/GaAs double quantum dots, *Solid State Communications* 117(7), 401-406, (2001).

[31] W. Sheng and J.-P. Leburton, Anomalous quantum-confined stark effects in stacked InAs/GaAs self-assembled quantum dots, *Phys. Rev. Lett.* 88, 167401, (2002)

[32] S. Taddei, M. Colocci, A. Vinattieri, F. Bogani, S. Franchi, P. Frigeri, L. Lazzarini and G. Salviati, Vertical coupling and transition energies in multilayer InAs/GaAs quantum-dot structures, *Phys. Rev. B* 62, 10220-10225,(2000).

[33] O. Voskoboynikov, C.P. Lee and O. Tretyak, Spin-orbit splitting in semiconductor quantum dots with a parabolic cofinement potential, *Phys. Rev. B* 63, 165306, (2001).

[34] O. Voskoboynikov, S.S. Liu and C.P. Lee, Spin-dependent electronic tunnelling at zero magnetic field, *Phys. Rev. B* 58(23), 15397-15400, (December 1998).

[35] W.Wang, T.-M. Hwang, J.-C. Jang, A second-order finite volume scheme for three dimensional truncated pyramidal quantum dot, *accepted Computer Physics Communications*

[36] Z.R. Wasilewski, S. Fafard and J.P. McCaffrey, Size and shape engineering of vertically stacked self-assembled quantum dots, *Journal of Crystal Growth* 201-202, 1131-1135, (1999).